THE ASTROPHYSICAL JOURNAL, 308:93–109, 1986 September 1

THE EVOLUTION OF THE COMPACT RADIO SOURCE IN 3C 345. I. VLBI OBSERVATIONS

J. A. BIRETTA, R. L. MOORE, AND M. H. COHEN
California Institute of Technology
Received 1985 October 7; accepted 1986 February 20

ABSTRACT

We present a systematic analysis of VLBI observations for the superluminal radio source 3C 345. Observation frequencies range from 2.3 to 89 GHz, and epochs are from 1979.25 through 1984.11. A newly ejected knot (C4) accelerates, changes position angle, and undergoes a large flux outburst. Older knots C2 and C3 have different speeds, little or no acceleration, and different position angles. The flux of C3 decays, and its spectrum steepens. Distances between the "core" and knots are larger at higher frequencies. The moving knots define an opening angle of $\sim 27°$ and show direct evidence of expansion. The counterjet to jet flux ratio is -0.007 ± 0.007.

Subject headings: quasars — radio sources: general — radio sources: variable

I. INTRODUCTION

The quasar 3C 345 is an interesting object at all frequencies. Ku, Helfand, and Lucy (1980) have detected it as a 2 keV X-ray source. At optical and infrared frequencies its flux varies by a factor of 5 on time scales of a few months, making it one of the most variable quasars (Grandi and Tifft 1974; Neugebauer *et al.* 1979; Pollock *et al.* 1979). The optical polarization is high and variable (Moore and Stockman 1981), and there is evidence for optical nebulosity (Hutchings, Crampton, and Campbell 1984). At radio frequencies it is one of the strongest compact sources, and the flux density varies by a factor of 2 on time scales of a few years at centimeter wavelengths. There is no evidence for low-frequency variability.

The radio structure of 3C 345 consists of a faint steep spectrum halo of diameter 20″ (Schilizzi and de Bruyn 1983), a steep spectrum jet 3″ long which terminates in a bright hot spot (Browne *et al.* 1982*b*), and a milli–arc second (mas) scale region which has a flat spectrum and dominates the flux above a few hundred MHz. Early evidence of superluminal motion in the compact structure was given by Cohen *et al.* (1976) and Wittels *et al.* (1976). Because of its brightness and high declination, it has become the best studied of the superluminal sources (Cohen and Unwin 1984). Unwin *et al.* (1983, hereinafter U83) have presented results of VLBI monitoring at two frequencies between 1979 and 1981. They give clear evidence for superluminal motion and for a relativistic Doppler factor significantly greater than unity, based on the internal proper motion and on the weakness of the inverse Compton X-ray flux. Recently Biretta *et al.* (1983) and Moore, Readhead, and Bååth (1983) have presented evidence for interesting kinematics of a newly ejected knot.

In this paper we present new VLBI observations from 1982 through 1984 and a systematic reanalysis of previously reported VLBI data since 1979 (Biretta *et al.* 1983; Cohen *et al.* 1983; Moore, Readhead, and Bååth 1983; Readhead *et al.* 1983; U83; Backer 1984). A total of 20 epochs are analyzed and presented. The observational and data reduction procedures are given in § II. Sections III and IV, respectively, describe qualitative and quantitative results. Important results are summarized in § V. A subsequent paper will present physical interpretations.

Throughout this paper we will use a redshift $z = 0.595$ (Burbidge 1965) and assume $H_0 = 100h$ km s^{-1} Mpc^{-1} and $q_0 = 0.5$. For a standard Friedmann cosmology 1.00 mas corresponds to $3.79h^{-1}$ pc. A proper motion of 1.00 mas yr^{-1} corresponds to $v/c = 19.7h^{-1}$. Quoted uncertainties are 1.0 σ.

II. OBSERVATIONS AND REDUCTIONS

Very Long Baseline Interferometric (VLBI) observations were made of 3C 345 at 2.3, 5.0, 10.7, and 22.2 GHz. Details of the epochs and antenna arrays are given in Table 1. About 12 hr of observation were obtained at each epoch. A bandwidth of 1.8 MHz was recorded using Mk II equipment (Clark 1973; Moran 1973). System temperatures were measured every hour at 2.3, 5.0, and 10.7 GHz, and every half-hour at 22.2 GHz. Antenna temperatures were also measured wherever possible.

The data were subsequently correlated at the CIT-JPL five station processor. Correlation amplitudes and phases were measured with the PHASOR fringe fitting program. For signal-to-noise ratios (S/N) less than 10 the amplitudes were corrected for the positive bias introduced by the Rice distribution and truncation (Linfield 1981). For S/N ≤ 3 the bias is difficult to correct, so the uncertainties for these data points were increased by a factor of 3. Correlation coefficients were converted to flux densities using the technique described by Cohen *et al.* (1975) and the flux scale of Baars *et al.* (1977). The 1982.42 data were processed at the MPIfR correlator at Bonn, West Germany. (Bååth *et al.* 1985). Visibility data at 89.0 GHz are from Backer (1984), and the observation procedure is described therein.

We have used both mapping and model fitting to derive information about the source structure from the visibility data. Mapping (Readhead and Wilkinson 1978) is used to obtain a qualitative description of the source structure. Mapping can render complex details of the source structure with only a crude starting model, but the resulting map is not unique when much of the (u, v) Fourier transform plane contains no data (Cornwell 1982*a*). Hence it is difficult to specify the uncertainties in parameters measured from the maps. For producing quantitative measurements with formal uncertainties we use model fitting (Simon 1983). It has the advantage that it produces a simplified description of the source with few free

TABLE 1

DETAILS OF ANTENNA ARRAYS USED IN OBSERVATIONS

Epoch	Frequency (GHz)	Antennas[a]	Beam Shape[b] (mas)	$\lambda/2D$ (min)[c] (mas)	f^{d}	p^{e}
1979.25	4.996	BGFOH	0.9 × 1.7	14	0.23	3
1979.44	10.651	BKGFO	0.4 × 0.8	11	0.28	3
1979.92	5.009	BKGFO	0.9 × 1.7	22	0.30	2
1980.52	10.651	BKGFO	0.4 × 0.8	4	0.32	1
1980.73	5.009	BKFO	0.9 × 1.7	8	0.28	2
1981.09	10.651	BKGFO	0.4 × 0.8	8	0.34	1
1981.25	22.231	BKGCYO	0.25 × 0.40	5	0.42	2
1981.63	4.989	BKGFO	0.9 × 1.7	22	0.37	3
1981.89	2.292	SJMGFAOH	2.6 × 2.1	45	0.55	1
1982.09	10.651	BKGCFO	0.4 × 0.8	16	0.43	1
1982.38	89.026	PLD	...	0.7	0.01	...
1982.42	22.231	RSKGYO	0.25 × 0.40	4	0.53	3
1982.56	4.990	BKGFO	0.9 × 1.7	14	0.41	0.5
1982.86	10.651	BFO	...	2	0.11	...
1983.09	22.231	BSKGYO	0.25 × 0.40	3	0.59	1
1983.10	10.651	BKGFOH	0.4 × 0.8	12	0.45	0.5
1983.57	4.990	BKGIFYOH	0.9 × 1.7	25	0.50	0.1
1983.76	22.231	BSKGYO	0.25 × 0.40	4	0.58	1
1984.09	22.231	BSKGNO	0.25 × 0.40	13	0.47	1
1984.11	10.651	BKGFOH	0.4 × 0.8	10	0.50	0.5

[a] Key.—B: Bonn 100 m. C: Algonquin 50 m. D: Hat Creek 6 m (millimeter dish). F: Fort Davis 26 m. G: NRAO Greenbank 43 m. H: Hat Creek 26 m. I: Iowa 18 m. J: Jodrell Bank 76 m. K: Haystack 37 m. L: OVRO 10 m. M: Madrid 64 m. N: NRL Maryland Point 26 m. O: OVRO 40 m. P: Kitt Peak 11 m. R: Crimea 22 m. S: Onsala 20 m. Y: VLA 25 m.

[b] Shape of central component of dirty beam assuming uniform weighting of data points in (u, v) plane. Note that a circular beam was actually used for the maps we display.

[c] Largest source scale to which interferometer is sensitive, estimated as $\lambda/2D$ for shortest baseline.

[d] Fraction of cells in gridded (u, v) plane which contain data. A filled aperture would have $f = 1$. See text.

[e] Percent of peak intensity level at which weak features in the map become unreliable.

parameters, and it is easy to estimate formal uncertainties due to missing (u, v) data, calibration problems, and so on. The disadvantage of model fitting is that the basic morphology of the source must be put in at the beginning of iteration, but this is not a serious drawback since maps are available to guide the choice of starting model.

a) Mapping Procedure

Maps were made from the visibility data for every epoch with four or more antennas. The procedure differs from that used previously and is diagramed in Figure 1. It iterates on nested loops of mapping and modeling, until convergence is achieved. It works only when the visibility function is reasonably well sampled, and we did not attempt it unless there were four or more antennas.

We begin by choosing a starting model and "self-calibrating" the visibility data (Cornwell and Wilkinson 1981). The starting model consists of either one or two Gaussian components and is obtained by fitting to the calibrated data. After self-calibration, the visibility data are Fourier transformed to produce a map, the map is CLEANed, and then the CLEAN components are used to self-calibrate the data again. These last three steps are repeated (loop A) until the self-calibration has converged and the fit to the (u, v) data ceases to improve. Loop A is typically iterated 4 times. During self-calibration, we permit antenna gains to vary on time scales of a few hours at 2.3, 5.0, and 10.7 GHz and on time scales of a few minutes at 22.2 GHz.

After convergence, the starting model and final map are compared. The starting model is then revised by adding components (if necessary) and refitting to the improved visibility

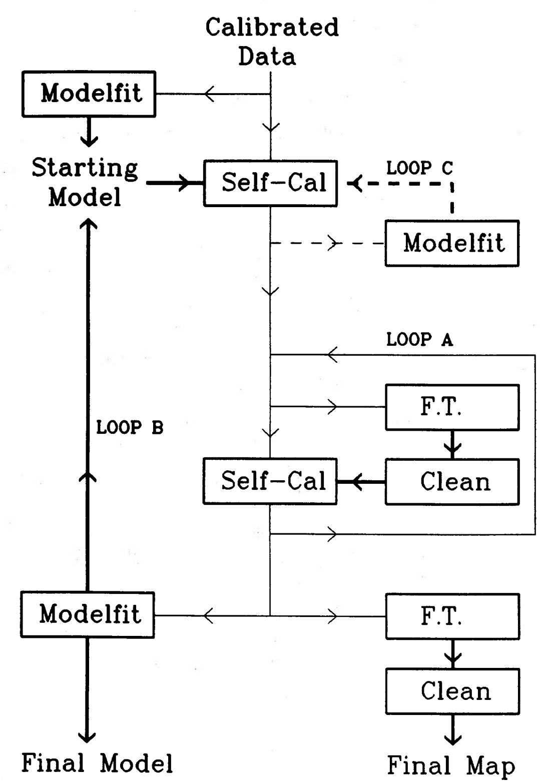

FIG. 1.—Diagram describing mapping procedure. "FT" stands for Fourier transform. Heavy lines represent paths involving image data, light lines represent visibility data.

data. This revised starting model then replaces the old starting model, and the entire mapping process is repeated beginning with the uncorrected visibility data (loop B). It is important to return to the original data regularly, since the self-calibration process can become unstable. Loop B is typically iterated 4 times. This method constantly improves the starting model for the mapping procedure (Pearson and Readhead 1984) and thus increases the dynamic range of the final map.

In cases where the *a priori* calibration or (u, v) coverage is poor, loop C is used to improve the calibration before mapping. That is, visibility corrections based on the starting model are generated; a new model is fitted to the data; then the new model is used to correct the visibilities, and so on.

Model fitting, as used in loops B and C, serves to reject unsatisfactory reconstructions of the source intensity distribution. Often CLEAN is used for this purpose, by either windowing or by excluding some of the CLEAN components, or both. Model fitting can perform this same function with the advantages that it (1) provides a good description of the source with very few free parameters, (2) provides strong rejection of spurious features, (3) can reject negative flux, (4) can include extended features of low surface brightness without introducing many free parameters, and (5) can include features away from the center of the image plane. Hence it is very attractive for the early iterations of self-calibration. Later self-calibration with maps is still necessary, since a simple model cannot render all the details of the source.

b) *Calculation of Models for Use in Quantitative Analysis*

We have fitted models to the final self-calibrated visibility functions for the purpose of deriving quantitative measurements. They consists of several optically thin, homogeneous spherical components, whose shape is invariant under rotation and relativistic transformation; this property will simplify later analyses. A typical map and model are shown in Figure 2.

Uncertainties in the model parameters were determined by the method of Arndt and MacGregor (1966). The uncertainty in a parameter was defined as the variation in that parameter which would cause the reduced χ^2 to increase by a factor $1 + 1/N$ when *all* other parameters were allowed to vary. For random errors with a Gaussian distribution N is the number of independent errors minus the number of fit parameters, and the method produces 1 σ uncertainties. For perfect data N would be simply the number of independent (u, v) points. However, calibration problems cause a correlation of the errors for data points adjacent in time. We assumed that the most serious errors in our data were due to antenna-dependent calibration problems having a 1 hr time scale. Hence $N \approx (12$ hr) $\times$ (1 independent error per hour) $\times$ (m) for 1 σ errors, where m is the number of antennas. In practice we computed 2.5 σ errors by setting $N = 12m/(2.5)^2$, and then divided the result by 2.5; this assumes that the fitting function is approximately linear and reduces numerical instabilities. This same method was used to determine whether a component should be included in the model; components were included only if their presence was significant at the 2.5 σ level. The method takes into account the quality of the (u, v) coverage; if a parameter is not well constrained by the (u, v) data, the χ^2 will be insensitive to variations in the parameter, and the estimated uncertainty will be large. Since the calibration errors may not have a Gaussian distribution function, and since the fitting function is not exactly linear, the uncertainties we give are only approximate.

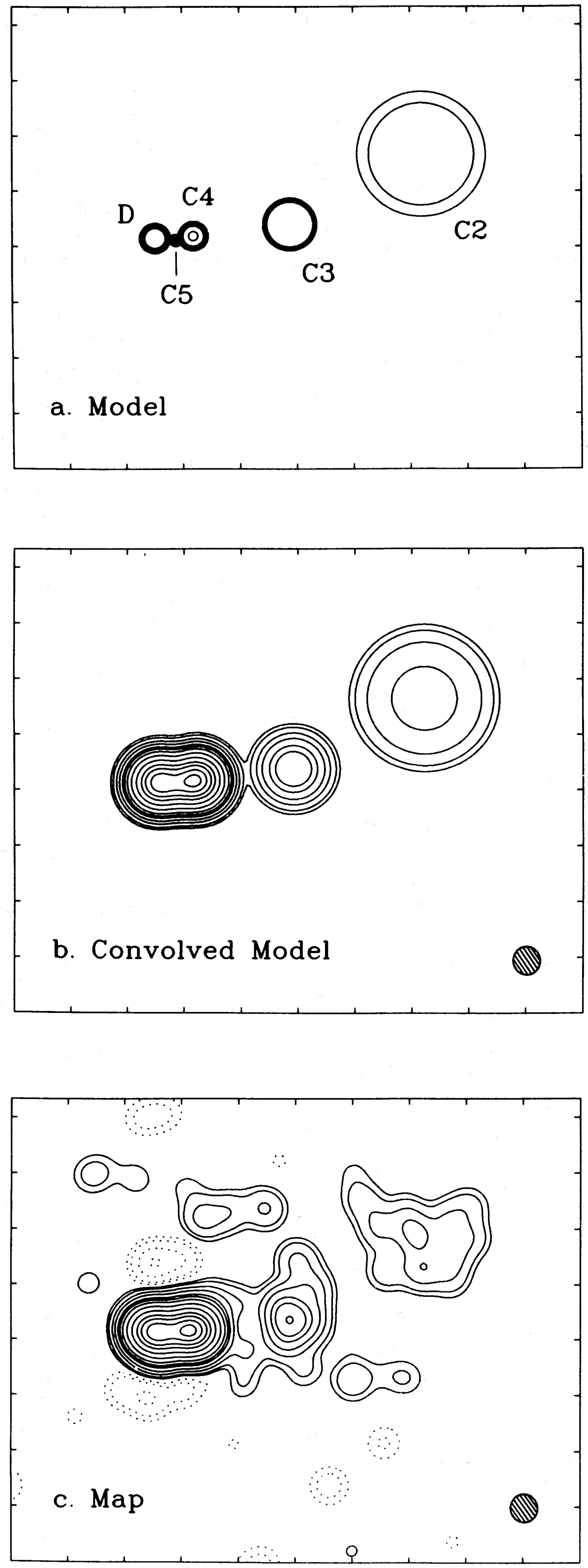

FIG. 2.—Contour plot of model and map for 1984.11 epoch at 10.7 GHz. Contours are at ± 0.1, ± 0.2, ± 0.5, ± 1, ± 2, ± 3, ± 5, ± 10, ± 20, ± 35, ± 50, ± 70, and ± 90 percent of the peak intensity. Shaded regions show FWHM of Gaussian convolving beam. (*a*) Model with no beam convolution. (*b*) Model convolved with 0.6 mas FWHM Gaussian function. (*c*) Map with 0.6 mas FWHM Gaussian CLEAN restoring beam.

The fluxes of the model components were adjusted so that

$$S_{\rm res} = S_{\rm total} - S_{\rm model}$$

would be constant from epoch to epoch, where $S_{\rm res}$ is the flux of components resolved by VLBI, $S_{\rm total}$ is the total source flux, and $S_{\rm model}$ is the total flux of model components D and C5–C2 (using the labeling convention of U83). The purpose of this adjustment is to remove epoch-to-epoch variations in the model fluxes which are caused by antenna and correlator calibration errors. It assumes that structures too large to be seen by VLBI have constant flux on time scale of a few years. The highest quality data are at 5.0 GHz, and for this frequency we set $S_{\rm res} = 1.02$ Jy at 5.0 GHz, the average value for the six epochs. This flux of 1.02 Jy may be broken up into a contribution of 0.55 Jy from structures resolved with MERLIN (Schilizzi and de Bruyn 1983; Browne *et al.* 1982*a*) and a contribution of 0.47 Jy which must be due to emission on scales between ~20 and 200 mas. For other frequencies, we assumed $S_{\rm res}$ had a spectral index of $\alpha = -1.0$ ($S_\nu \propto \nu^\alpha$) (Schilizzi and de Bruyn 1983; Browne *et al.* 1982*a*). At 10.7, 22.2, and 89.0 GHz, components C3 and C2 do not appear in the model for some epochs. In these cases we extrapolated the 5.0 GHz flux of C2 and C3 assuming $\alpha = -1.0$ and included this flux in $S_{\rm model}$. The corrections to the model flux had a median value of 5%; the largest correction was 50% for the 1983.09 data at 22 GHz. At any given frequency, the scale size sampled by the shortest baseline varies from epoch to epoch (col. [5] of Table 1). This variation has no appreciable effect on the correction, since scale sizes between ~5 and ~20 mas contain little flux.

c) Reliability of the Maps and Models

The reliability of our reconstruction of the source intensity distribution is limited by incomplete (u, v) coverage, by calibration errors, and by thermal noise in the antenna systems. The most serious uncertainties are those caused by incomplete (u, v) coverage. The fractions f of the gridded (u, v) plane which contain data are given in Table 1 for each epoch. (For the purpose of gridding, the map size was taken to be 200 mas/ν(GHz) or 256 × 256 pixels which is the size typically used during CLEANing). The f-values are typically 0.5 or less, so that simple Fourier transformation of the visibility data cannot yield a unique representation of the source.

During mapping we used two constraints which reduce the ambiguity caused by the missing data: (1) the map intensity must be positive and (2) the assumption that most of the flux is in a small region near map center. These assumptions greatly reduce the number of possible intensity distributions consistent with the observed data, but still do not guarantee a unique map. No algorithm has yet been found for quantifying this uncertainty (Cornwell 1982*b*). For lack of such an algorithm, we define the uncertainty as the intensity level of weak features thought to be spurious. These are given in Table 1 as a fraction of the peak intensity. Uncertainties estimated this way are only a rough guideline, and apply only to low-intensity regions of the map.

The factors listed above also limit the reliability of the models, but they were taken into account when estimating uncertainties on the model parameters. Models also have an additional uncertainty: the choice of model itself. In all cases we chose the number and locations of components to resemble the map, so the basic structure of the model is justified by the appearance of the map. This uncertainty would be important only if the gross structures in the map were incorrect, and this seems very unlikely since they are the same from epoch to epoch and at different frequencies.

It is possible that details of the model, such as the choice of component shape (optically thin spheres) could be incorrect. This has little effect on the results. If we had used optically thick spheres, instead of optically thin ones, the models would remain unchanged except for the component diameters, which would decrease by a factor of 0.84. If Gaussian components were used, FWHM values equal to 0.594 (sphere diameter) would have been obtained. In the one case where a component appears to be strongly noncircular (C4 at epoch 1984.09), the model we use and one with an elliptical component both give the same flux and mean diameter.

One final problem which might occur is in the comparison of models at different frequencies. In some cases a low-frequency model does not have all the components seen at a higher frequency. In these cases additional fits were made, with the same model being used at both frequencies. In no case were the results significantly different from the models we present.

d) Comparison with Analysis Methods of Unwin et al.

Our quantitative analysis is based on models which are fitted to the visibility data, while the U83 analysis is based on contour plots of maps. In some cases these two methods produce systematically different results.

Our component separations are in good agreement with theirs at 10.7 GHz, but they obtain systematically larger separations than ours at 5.0 GHz. This is most likely due to their use of two different methods at the two frequencies. At 10.7 GHz components D and C3 were well separated and they take the centroid of C3 as the center of the highest few contours. However, at 5.0 GHz D and C3 are blended together on the maps, so that the centroid of C3 was taken as the point one-half beam FWHM east of the western half-intensity point. But in cases where the components are extended, the centroid will occur more than 0.5 FWHM away from the western half-intensity point. Hence their centroids for C3 are too far west at 5.0 GHz, and they obtain separations between D and C3 which are too large.

We measure component sizes as the diameter of the spherical model component, while U83 measure directly from the maps and allow for the size of the restoring beam. We find that C2 and C3 are resolved, while U83 find that "few components are significantly resolved." The two techniques were tested by applying them to data for an artificial source which resembled 3C 345 and had known component sizes. Different sets of artificial data were generated assuming four, six, and eight antennas; thermal noise and realistic calibration errors were included. The artificial data were then hybrid mapped and self-calibrated, and component sizes were measured using the above techniques. Measurement by model fitting was found to give sizes in the range 0.9 to 1.3 times the actual size, while measurement from the maps gave sizes 0.3 to 1.0 times the actual size. Hence, sizes determined by measurement from maps appear to be biased toward small sizes. This may be caused by the map being poorly constrained, or by the tendency of CLEAN to produce overly sharp features.

Our fluxes agree with those of U83 for components much smaller than the beam size, but for extended components their fluxes tend to be smaller than ours. U83 measure the peak brightness on the map and then multiply this by the beam area to obtain fluxes, thereby assuming the components to be unresolved. Their assumption that the components are unresolved causes them to obtain low fluxes for resolved components. We simply use the flux found in the model-fitting procedure.

III. QUALITATIVE RESULTS

The maps are presented in Figure 3. Earlier versions of several maps have been presented elsewhere (Cohen *et al.* 1983; U83; Readhead *et al.* 1983; Moore, Readhead, and Bååth 1983; Biretta *et al.* 1983; Bååth *et al.* 1986, in preparation), but in all these cases the data have been recalibrated, remapped, and modeled as described above. Model parameters are presented in subsequent figures and are listed elsewhere in tabular form (Biretta 1985). These maps and models form the largest set of homogeneous data assembled for a compact radio source.

All the maps show a basic "core-jet" morphology (Readhead and Pearson 1982) with bright knots in the jet. We will use the notation of U83 for labeling the "knots" and the "core."

The 2.3 GHz map shows components C1, C2, and C3. Component C3 is the brightest component, while C1 is weak and extended. Component D appears as an eastern extension from C3.

The 5.0 GHz maps clearly show components C2 and C3 separating from component D.[1] Component D is the brightest, with C3 and C2 being progressively weaker in surface brightness. The component sizes (FWHM) progressively increase from D to C3 to C2. The 1983.57 observations involved more antennas than any other epoch and the maps has a high dynamic range. The ratio of peak brightness to rms noise away from the map center is ~2700:1, which is the highest value ever attained for a VLBI map. The measured noise level in the map is 2.7 ± 0.3 mJy per beam, which is close to the value of 1.8 mJy per beam expected for the antennas and receivers used in the observations. This map shows only weak structures beyond C2 and no evidence of a counterjet (see § IV*c*).

The 10.7 GHz maps show that C2 and C3 move relative to D in a way similar to that seen at 5.0 GHz. In 1981 component D begins to show an extension which is labeled C4 (Biretta *et al.* 1983; Moore, Readhead, and Bååth 1983). This new component then moves away from D and changes position angle from $-135°$ to $-86°$. Two of the maps (1982.09 and 1983.10) show evidence for a weak component between C3 and C4 which we have labeled C3.5. The inclusion of this component significantly improved the fit of the model to the visibility data.

At 22.2 GHz maps plainly show component C4 changing position angle and separating from D. They also show significant evolution of C4; initially it is much weaker than D, but at later epochs it is of comparable brightness. At the last epoch C4 shows elongation along P.A. = $-60°$. Component D itself appears to have a weak extension after 1983, which can be seen once C4 is sufficiently far away. Although the nature of this extension is not yet clear, we have included it in the models since it significantly improves the fit, and we label it C5. The three maps after 1983 all show a weak feature 0.7 mas northeast of D, but this feature was not significant at the 2.5 σ in any one data set and was therefore not included in the models.

[1] Bartel *et al.* (1984) have given evidence that D is nearly stationary on the sky; its proper motion relative to NRAO 512 is 0.02 ± 0.02 mas yr^{-1} on a 10 yr time scale.

IV. QUANTITATIVE RESULTS

a) Positions and Proper Motions of Component Centroids

The positions of the centroids of knots C2, C3, C4, and C5 on the sky relative to component D are shown in Figure 4*a*. An enlargement of the region near D is shown in Figure 4*b*. We define $\boldsymbol{r}$ to be a vector from the centroid of D to the component centroid, with $r = |\boldsymbol{r}|$. During the period 1979 to 1984 C2 moved from a radial distance $r \approx 3.6$ to 5.9 mas, C3 moved from $r \approx 1.2$ to 2.9 mas, and C4 moved from $r \approx 0.2$ to 0.9 mas. To derive proper motions for the components, functions of the form $\boldsymbol{r}(t) = \boldsymbol{r}(t_0) + (d\boldsymbol{r}/dt)t$ were fitted to the data. The position $\boldsymbol{r}(t_0)$ for some fiducial epoch t_0 and the proper motion $d\boldsymbol{r}/dt$ are given in Table 2. We will treat each frequency separately so as to avoid complications caused by spectral index gradients.

Components C2 and C3 have significantly different proper motions. Component C2 has the highest proper motion of all the components, $|d\boldsymbol{r}/dt| = 0.48 \pm 0.02$ mas yr^{-1}, while C3 has $|d\boldsymbol{r}/dt| = 0.30 \pm 0.01$ mas yr^{-1} (Figs. 5*a* and 5*b*). There is no significant difference in the proper motions derived at 5.0 and 10.7 GHz for these components. Both C2 and C3 have little or no acceleration; the formal values of the radial acceleration (d^2r/dt^2) are 0.08 ± 0.11 and 0.01 ± 0.04 mas yr^{-2}, respectively, at 5.0 GHz. The uncertainties allow either constant velocity or a small acceleration sufficient to give C3 the same speed as C2, when it has moved to C2's present position. Similar results have been obtained for 3C 120 (Walker *et al.* 1984) and 3C 273 (Unwin *et al.* 1985) in that components well separated from the "core" appear to have little or no acceleration.

Component C4 first appears near the core with a small proper motion $|d\boldsymbol{r}/dt| \approx 0.07$, but as shown in Figure 5*c* its proper motion increases to ~0.3 mas yr^{-1} by 1984. This speed is similar to that of C3. This observed acceleration cannot be an artifact of poor resolution because (1) if there were no acceleration, backward extrapolation of the 1983 motion would put the centroid of C4 coincident with the centroid of D at 1981.1,

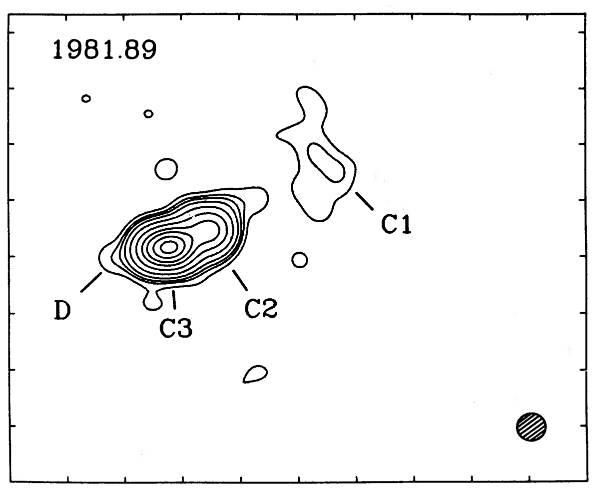

FIG. 3*a*

FIG. 3.—Contour plots of hybrid maps. North is at top, and east is at left. Contours are at ±0.05, ±0.1, ±0.2, ±0.3, ±0.5, ±1, ±2, ±3, ±5, ±10, ±20, ±35, ±50, ±70, and ±90 percent of the peak intensity. In most cases some of the lower contours have been omitted for clarity. Shaded areas represent FWHM of Gaussian CLEAN restoring beam. (*a*) 2.3 GHz map. Tick marks are at 4.8 mas spacing. Lowest contour is ±1%. Beam FWHM is 2.4 mas.

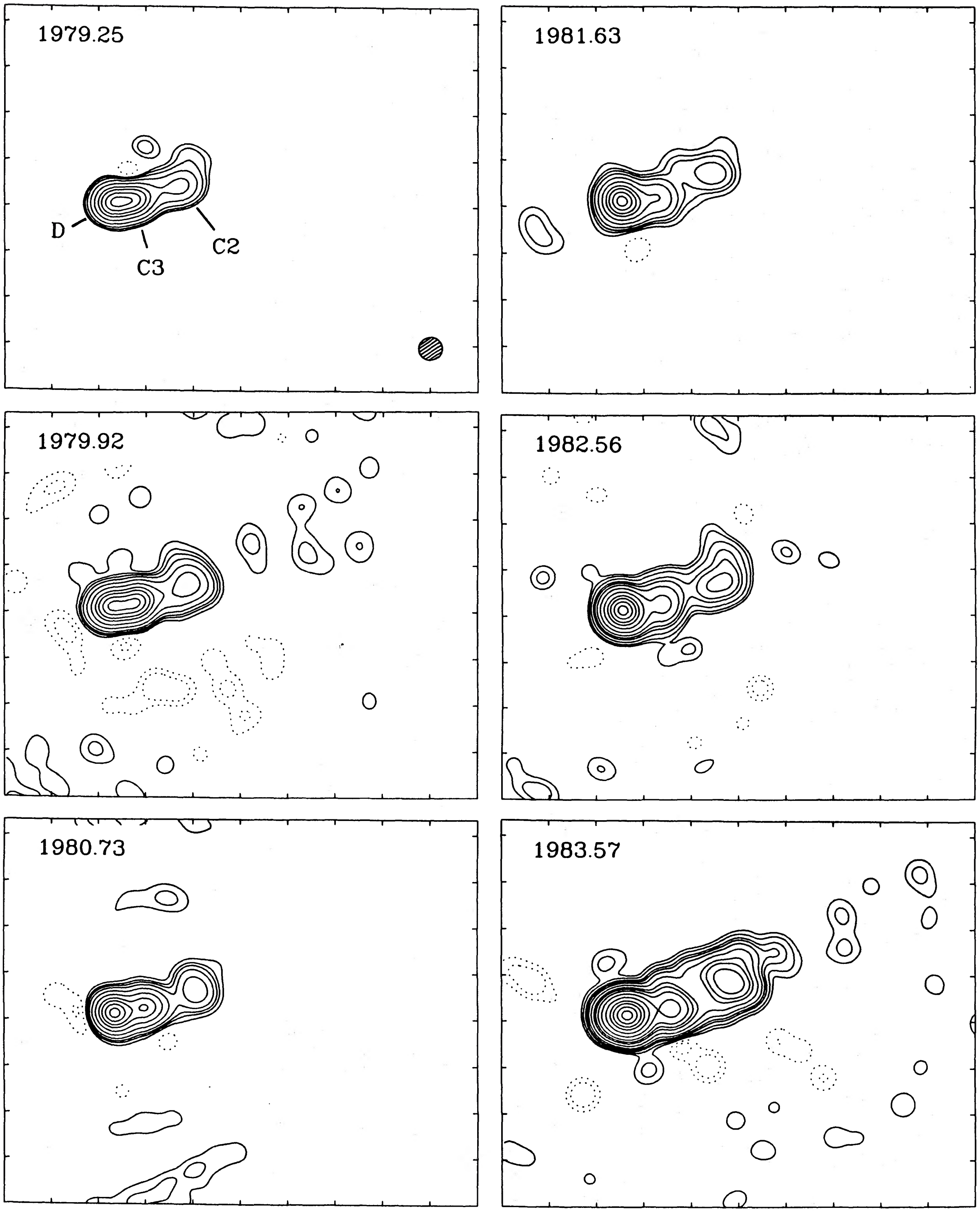

FIG. 3*b*.—5.0 GHz maps. Tick marks are at 2.4 spacing. Lowest contours are ±1% except for 1979.25, which is ±2%, 1982.56, which is ±0.3%, and 1983.57, which is ±0.05%. Beam FWHM is 1.2 mas.

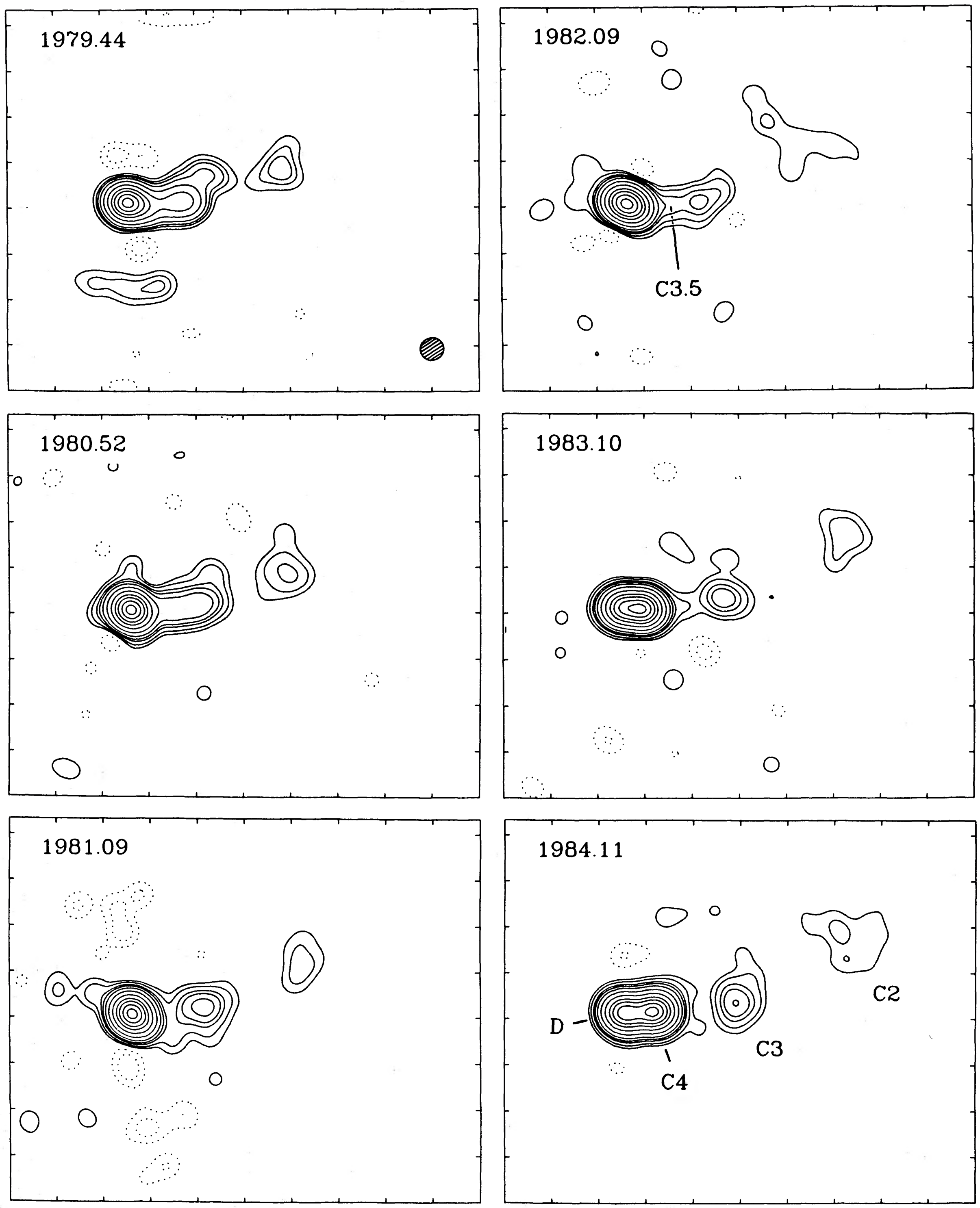

FIG. 3c.—10.7 GHz maps. Tick marks are at 1.2 mas spacing. Lowest contours are ±0.5% except for 1979.44 which is ±1%. Beam FWHM is 0.6 mas.

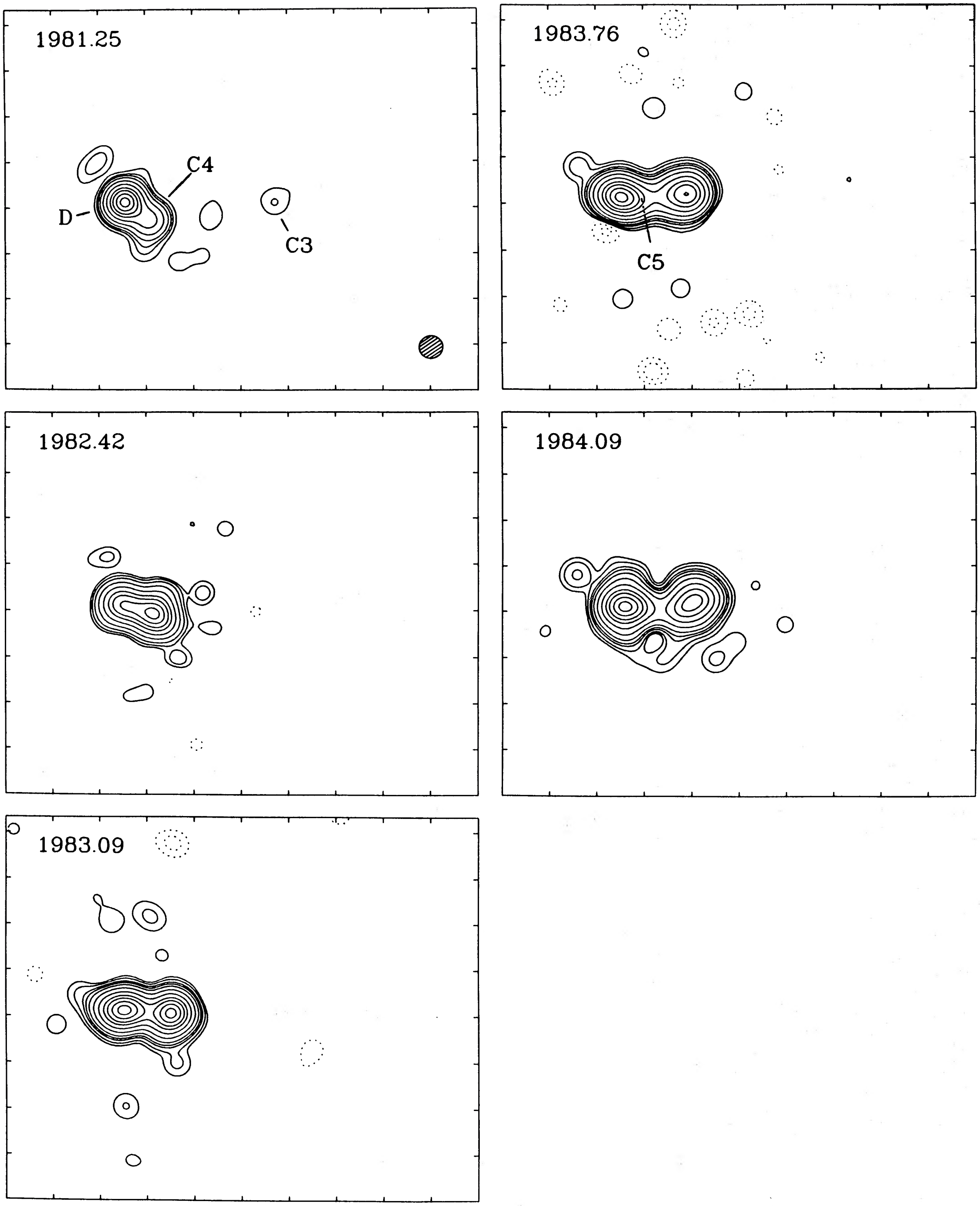

FIG. 3d.—22.2 GHz maps. Tick marks are at 0.6 mas spacing. Lowest contours are ±0.5% except for 1981.25, which is ±1%, and 1982.42, which is ±2%. Beam FWHM is 0.3 mas.

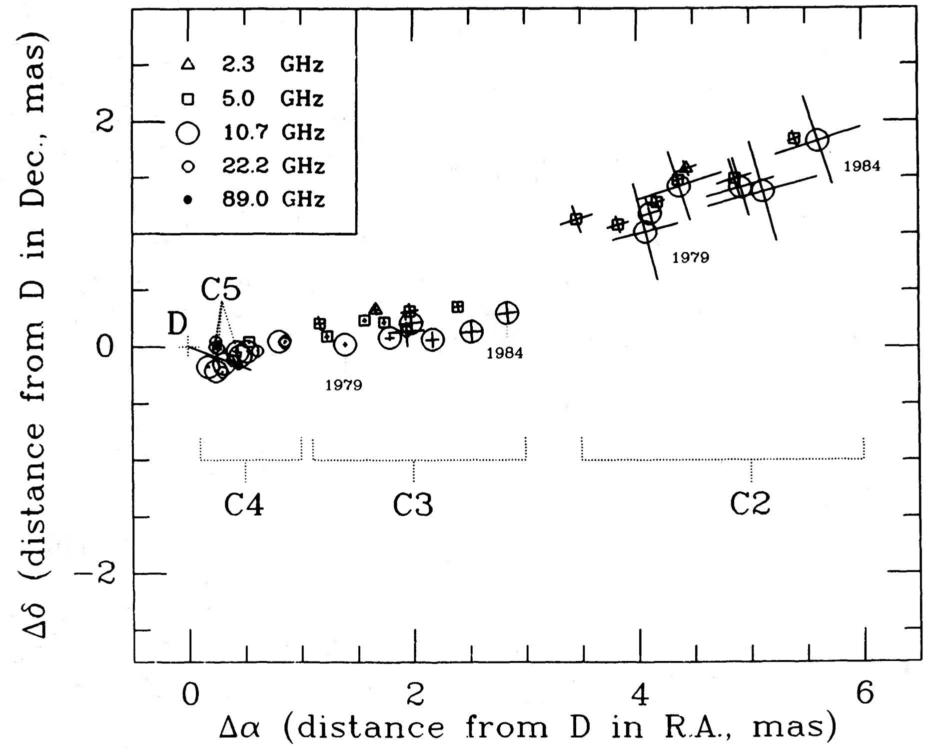

FIG. 4*a*

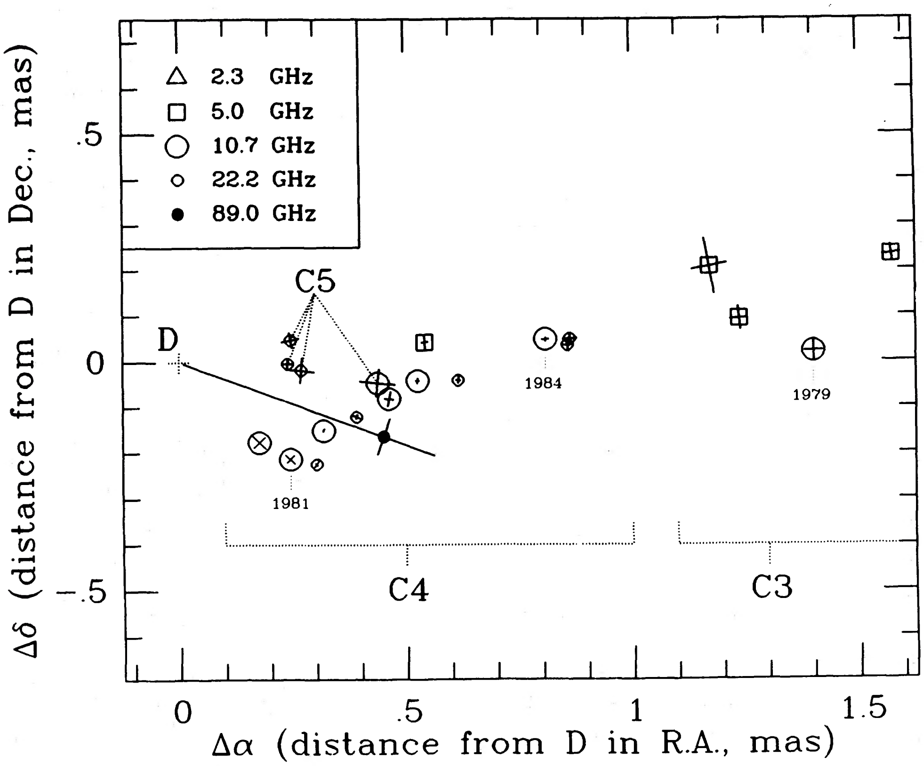

FIG. 4*b*

FIG. 4.—Positions of the centroids of components C5, C4, C3, and C2 relative to component D. Approximate epochs are shown for a few 10.7 GHz data points. (*a*) Data for all components. (*b*) Enlargement of region near D.

TABLE 2

PARAMETERS DESCRIBING POSITIONS AND PROPER MOTIONS OF C1, C2, C3, AND C4 RELATIVE TO *D*

				$r(t_0)$		dr/dt			
COMPONENT	ν (GHz)	EPOCHS USED	t_0	Magnitude (mas)	Direction P.A.	Magnitude (mas yr^{-1})	Direction P.A.	d^2r/dt^2 (mas yr^{-2})	d(P.A.)$/dt$ (deg yr^{-1})
C1..............	2.3	1981.89	1981.89	15.5 ± 1.9	$-64° \pm 18°$	...	...	...	...
C2..............	2.3	1981.89	1982	(4.76 ± 0.10)	(-70.4 ± 0.9)	...	...	...	...
	5.0	All	1982	4.89 ± 0.03	-71.9 ± 0.4	0.48 ± 0.02	$-66°.7 \pm 2°.5$	0.08 ± 0.11	0.59 ± 0.28
	10.7	All	1982	4.94 ± 0.13	-73.5 ± 1.5	0.41 ± 0.09	-68 ± 7	0.23 ± 0.36	0.4 ± 1.0
C3..............	2.3	1981.89	1982	(1.73 ± 0.04)	(-78.9 ± 1.4)	...	...	...	...
	5.0	All	1982	1.91 ± 0.02	-82.2 ± 0.4	0.298 ± 0.010	-78.7 ± 2.3	0.01 ± 0.04	0.45 ± 0.33
	10.7	All	1982	2.21 ± 0.03	-86.5 ± 0.7	0.312 ± 0.013	-81.5 ± 2.8	-0.03 ± 0.06	0.82 ± 0.38
C4..............	5.0	1983.57	1983.5	(0.524 ± 0.009)	(-86.1 ± 1.6)	...	...	...	...
	10.7	1982.86–1984.11	1983.5	0.640 ± 0.004	-91.6 ± 0.4	0.295 ± 0.009	-71.7 ± 1.5	...	8.3 ± 0.7
	22.2	1983.09–1984.09	1983.5	0.751 ± 0.005	-90.3 ± 0.4	0.330 ± 0.013	-71.3 ± 2.2	...	7.7 ± 1.0
C4..............	10.7	1981.09–1982.09	1982	0.350 ± 0.002	-116.7 ± 0.6	0.096 ± 0.018	-49 ± 7	...	15.7 ± 2.1
	22.2	1981.25–1982.42	1982	0.398 ± 0.005	-114.1 ± 0.7	0.066 ± 0.012	-49.4 ± 3.2	...	16.6 ± 1.2

NOTE.—Values in parentheses are extrapolations based on dr/dt at a different frequency.

but C4 clearly appears in maps near that epoch. (2) Both the 10.7 and 22.2 GHz data give similar velocities even though the resolutions differ by a factor of 2. It also accelerates in the sense that the direction of the velocity vector changes from approximately $-116°$ to approximately $-90°$ (Table 2, Fig. 4*b*). It is not clear whether these observed accelerations are instantaneous or occur over several months. Early evidence for this acceleration is described by Biretta *et al.* (1983) and Moore, Readhead, and Bååth (1983). The proper motion we obtain for 1982 is smaller than that given by Moore *et al.* (1983); the discrepancy arises from their use of different analysis methods on the 1981.25 and 1982.42 data.

These data for C2, C3, and C4 provide clear evidence for different components having different proper motions in a superluminal radio source. The only other evidence for this is given by Walker *et al.* (1984) for 3C 120.

The data for C4 also constitute the first unambiguous evidence yet found for acceleration. Cohen *et al.* (1983) have given some evidence for acceleration of C2 in this source based on comparison of early models from 1971 through 1974, with maps from 1979 through 1982. Early papers (Cohen *et al.* 1976; Wittels *et al.* 1976) also give evidence for acceleration of a component which may have been C2.

Figure 4 shows that the position angle of the knots increases monotonically with distance. Component C4 moves from P.A. $= -135°$ to $-87°$, while C3, C2, and C1 are at $-86°$, $-74°$, and $-64°$, respectively. The large-scale jet continues the curvature, changing from P.A. $= -38°$ to P.A. $= -32°$ between radii 1″ and 3″ (Browne *et al.* 1982*b*). This has been the subject of speculation about bent jets (Readhead *et al.* 1978). C4 clearly changes position angle between 1981 and 1983, but there is only marginal evidence that C3 and C2 change position angles with time (Table 2). In a few years C3 should overtake the earliest radii of C2, and then it should become clear whether their centroids are moving on different tracks.

The distances between the "core" component D and the knots C3 and C4 are larger at higher frequencies due to spectral index gradients. This can be seen in Figures 5*b* and 5*c*. Values of $r(t_0, \nu) - r(t_0, 10.7\ \mathrm{GHz})$ are given in Table 3. The effect is most significant for components C3 and C4. Since our data lack absolute positions, it is not possible to tell if the gradients occur in the "core," in the knots, or both. The shift between 5.0 and 10.7 GHz for component C3 (Fig. 5*b*) is different from the shift seen for C4 at 1983.57. This suggests that some of the effect is due to spectral index gradients in the C components.

Component C3.5 is a weak component which is seen at high frequencies prior to 1984. Its mean position angle of $-101° \pm 7°$ is consistent with other components at similar radii. But its proper motion $|dr/dt| \approx 0.14$ mas yr^{-1} appears to be slower than either C3 or C4 when at similar radii.

Component C5 is a weak extension from component D which is seen in 1983 and 1984. Its distance and position angle from D average ~ 0.25 mas and $-90°$ at 22.2 GHz. The position angle is quite different from that at which C4 first appeared, which suggests there is no single track near the core which component centroids follow. It has no proper motion; the formal value is $|dr/dt| = 0.00 \pm 0.03$ mas yr^{-1}. Future observations should reveal whether C5 begins to move like the other C components, or whether it has a different nature.

b) *Component Fluxes*

Component fluxes are plotted against epoch in Figure 6. To estimate time scales for flux variations we have fitted functions of the form

$$S(t) = S(1982.0)\ \exp\left[(t - 1982.0)/\tau\right]$$

to data for components C2, C3, C3.5, and C4 with results in Table 4. The spectra of components are plotted in Figure 7.

TABLE 3

FREQUENCY-DEPENDENT SHIFT IN COMPONENT POSITION

$r(t_0, \nu) - r(t_0, 10.7\ \mathrm{GHz})$

		FREQUENCY (GHz)			
COMPONENT	t	2.3	5.0	10.7	22.2
C2.........	1982	-0.18 ± 0.16	-0.05 ± 0.13	0	...
C3.........	1982	-0.48 ± 0.05	-0.30 ± 0.04	0	...
C4.........	1982	...	...	0	$+0.048 \pm 0.005$
	1983.5	...	-0.12 ± 0.01	0	$+0.111 \pm 0.007$

NOTE.—$r(t_0, \nu) - r(t_0, 10.7\ \mathrm{GHz})$ is in mas.

1986ApJ...308...93B

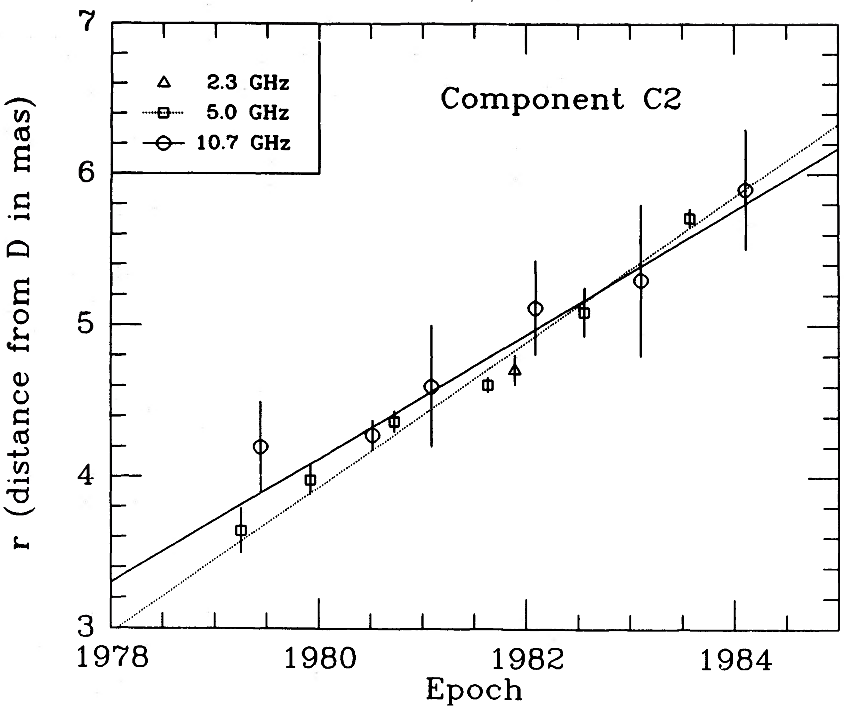

FIG. 5a

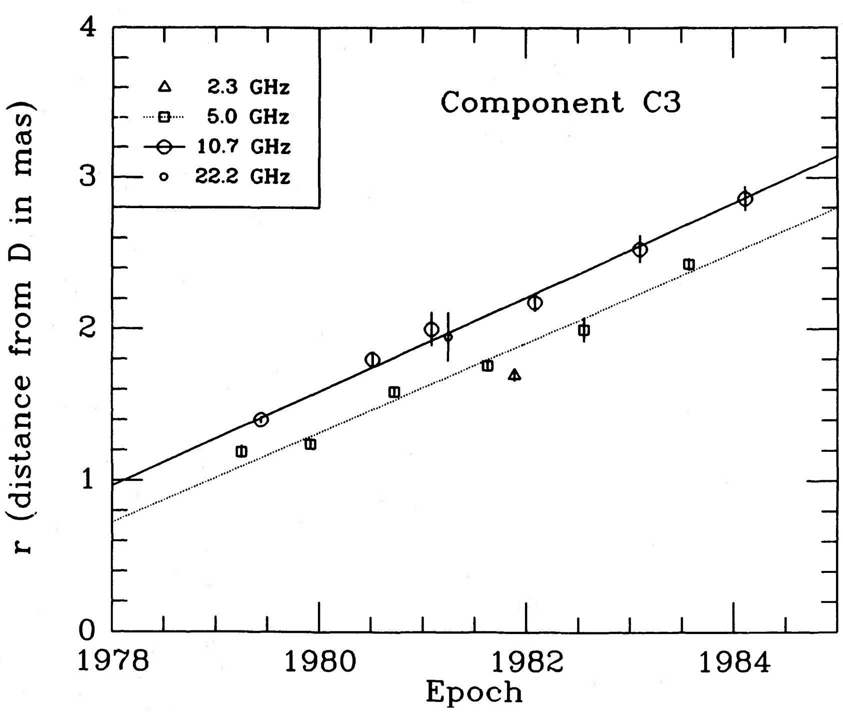

FIG. 5b

FIG. 5.—Radial distance $r = |\boldsymbol{r}|$ of component centroid from D vs. epoch. (*a*) Component C2. Lines fitted to 5.0 and 10.7 GHz data have slopes of 0.48 ± 0.02 and 0.41 ± 0.09 mas yr^{-1}, respectively. (*b*) Component C3. Lines fitted to 5.0 and 10.7 GHz data have slopes of 0.297 ± 0.010 and 0.311 ± 0.013 mas yr^{-1}, respectively.

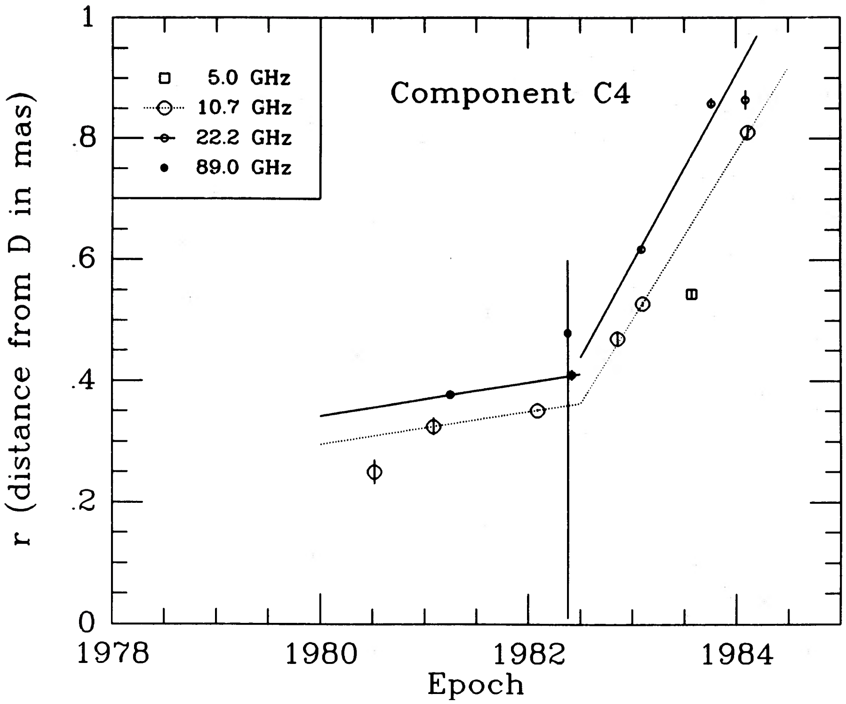

FIG. 5*c*.—Component C4. Lines fitted to 1981–1982 data have slopes of 0.027 ± 0.014 and 0.028 ± 0.008 mas yr^{-1}, respectively at 10.7 and 22.2 GHz. For 1983–1984 data the slopes are 0.277 ± 0.008 and 0.312 ± 0.012 mas yr^{-1}, respectively.

The fluxes for component C2 are shown in Figure 6*a*. At 10.7 GHz the large positive uncertainties are due to a lack of short spacings in the (u, v) plane. The spectrum is straight from 2.3 to 10.7 GHz, with $\alpha = -0.59 \pm 0.08$.

Figure 6*b* shows the data for component C3. The spectral index between 2.3 and 5.0 GHz is -0.37 ± 0.14. At higher frequencies it is appreciably steeper, $\alpha = -0.81 \pm 0.07$ between 5.0 and 22.2 GHz. The flux decays slightly faster at 10.7 GHz (4.3 ± 0.5 yr) than at 5.0 GHz (6.6 ± 0.5 yr), so that the spectral index steepens at a rate $d\alpha/dt = -0.11 \pm 0.04$ yr^{-1}.

Component C3.5 is a weak component, and it appears to decay more rapidly than any of the other components. Its flux decays with a time scale of 2.3 ± 0.4 yr, while the others have time scales of 4–6 yr at 10.7 GHz.

TABLE 4

RESULTS OF FITTING EXPONENTIAL LIGHT CURVES TO OBSERVED COMPONENT FLUXES

Component	Epochs Used	Frequency (GHz)	S(1982.0) (Jy)	τ (yr)
C2..............	79.25–83.57	5.0	1.09 ± 0.04	$< -15 \quad > 11$
	79.44–84.11	10.7	0.83 ± 0.14	$< -3 \quad > 3$
C3..............	79.25–83.57	5.0	1.82 ± 0.04	-6.2 ± 0.6
	79.44–84.11	10.7	0.91 ± 0.06	-3.7 ± 0.4
C3.5............	7.944–83.10	10.7	0.44 ± 0.05	-2.3 ± 0.4
C4..............	80.52–82.86	10.7	5.96 ± 0.24	2.2 ± 0.3
	77.9 –82.42	22.2	5.59 ± 0.16	1.53 ± 0.10
	82.86–84.11	10.7	8.90 ± 0.91	-4.8 ± 1.2
	82.42–84.09	22.2	8.22 ± 0.36	-3.8 ± 0.4

NOTE.—Fluxes for fiducial epoch 1982.0 and time scales for variation by factor e are given. All quantities are in the observer's frame of reference.

Component C4 undergoes a large flux outburst as it moves away from the "core" (Fig. 6*c*). At 22.2 GHz the flux of C4 rises from ≤ 1 Jy in 1978 to a peak of ~ 7.5 Jy at epoch 1982.4; it then decays more slowly to ~ 5 Jy by 1984. Similar variations are seen at 10.7 GHz. The time scale for the rise is 1.5 yr at 22.2 GHz, and somewhat longer, 2.2 yr, at 10.7 GHz. The decay time scales are ~ 4 yr. Because of the infrequent sampling it is not clear whether the fluxes at 10.7 and 22.2 GHz peak at the same opoch; any delay between the peaks could not exceed 1.5 yr.

The largest total flux outburst ever seen in 3C 345 began about 1979 (U83) and peaked near epoch 1981.6 at frequencies above 8 GHz (Feldman, MacLeod, and Andrew 1981; Biretta 1985). Component C4 is largely responsible for this outburst. This is the first example where an outburst occurs after a superluminal component is appreciably separated from the "core." A similar correlation between a total flux outburst and the appearance of a new component has been seen in BL Lac (Aller and Aller 1984; Mutel and Phillips 1984).

Below 10.7 GHz the spectrum of C4 rises with $\alpha \leq 0.8$ (Fig. 7). Between 10.7 and 22.2 GHz the spectral index varies between -0.30 and -0.14; it is interesting that the index at these frequencies varies so little while the flux doubles and then decreases. Above 22.2 GHz the spectral index is not well determined.

Component C5 is a westward extension from D which is evident after 1983.0. Its flux is near 1.5 Jy, and its spectrum is flat with $\alpha = -0.10 \pm 0.09$ between 10.7 and 22.2 GHz.

Component D is often blended with new components at low frequencies, but is seen separately at high frequencies where there is sufficient angular resolution. In order to consider the same physical region when comparing fluxes at different frequencies, we must combine the flux of D with that of C5 and C4.

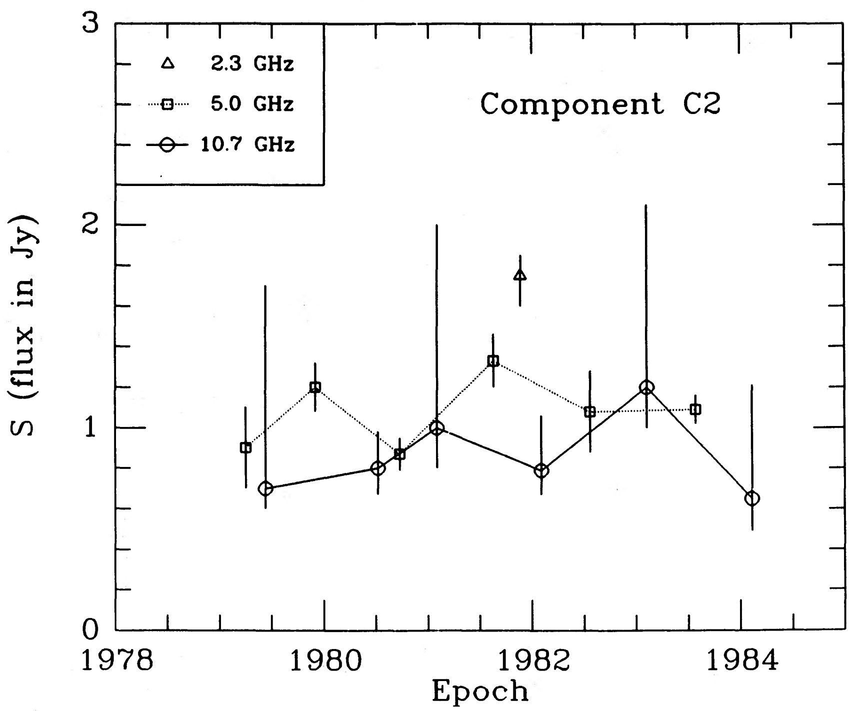

FIG. 6*a*

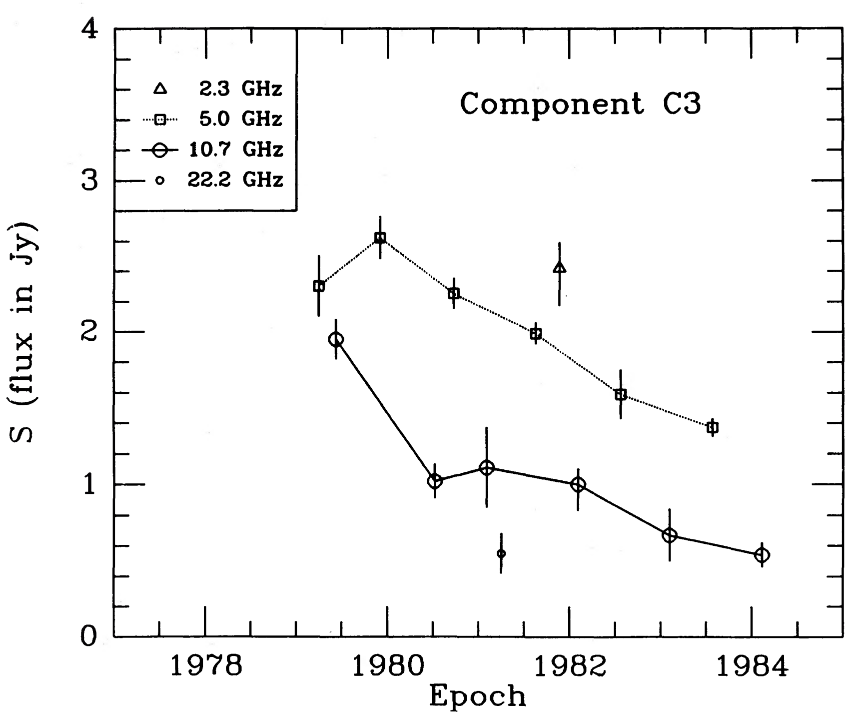

FIG. 6*b*

FIG. 6.—Fluxes of components vs. epoch. Lines have been drawn connecting data at the same frequency. (*a*) Component C2. (*b*) Component C3.

1986ApJ...308...93B

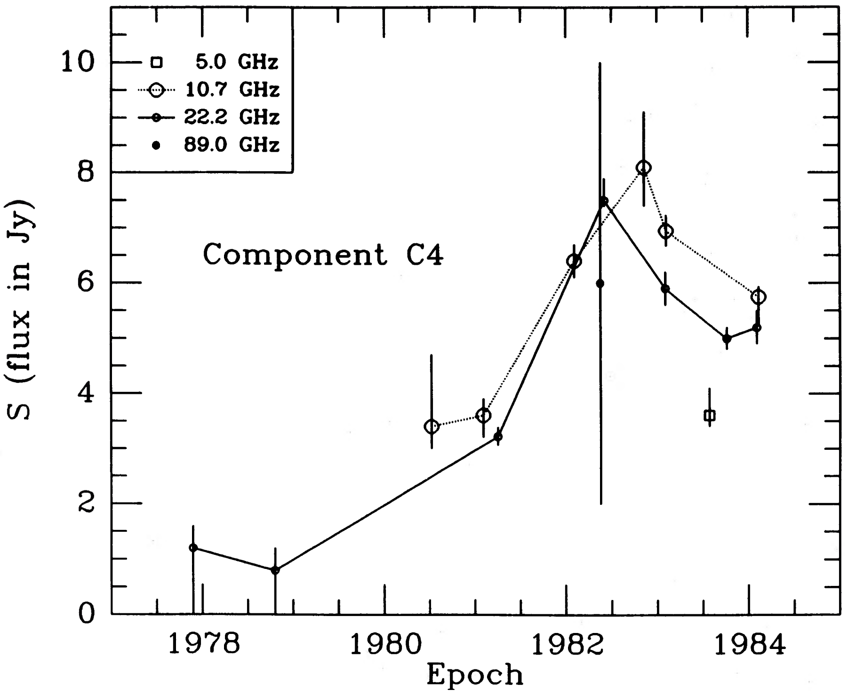

FIG. 6c

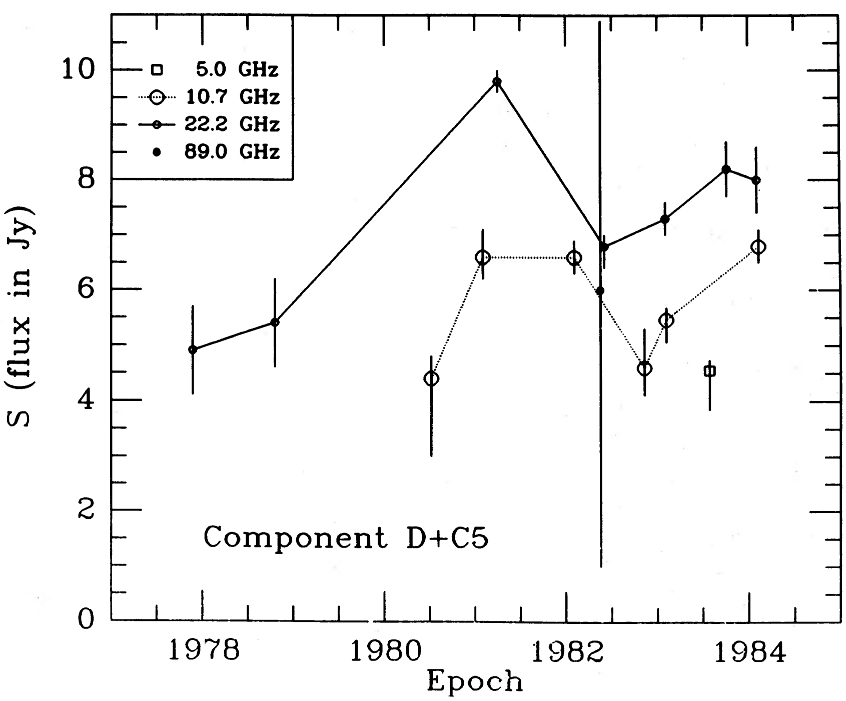

FIG. 6d

FIG. 6.—(c) Component C4. The 1979.9 and 1978.8 epoch data are from Bååth *et al.* (1981). (d) Components D + C5. (e) Components D + C5 + C4.

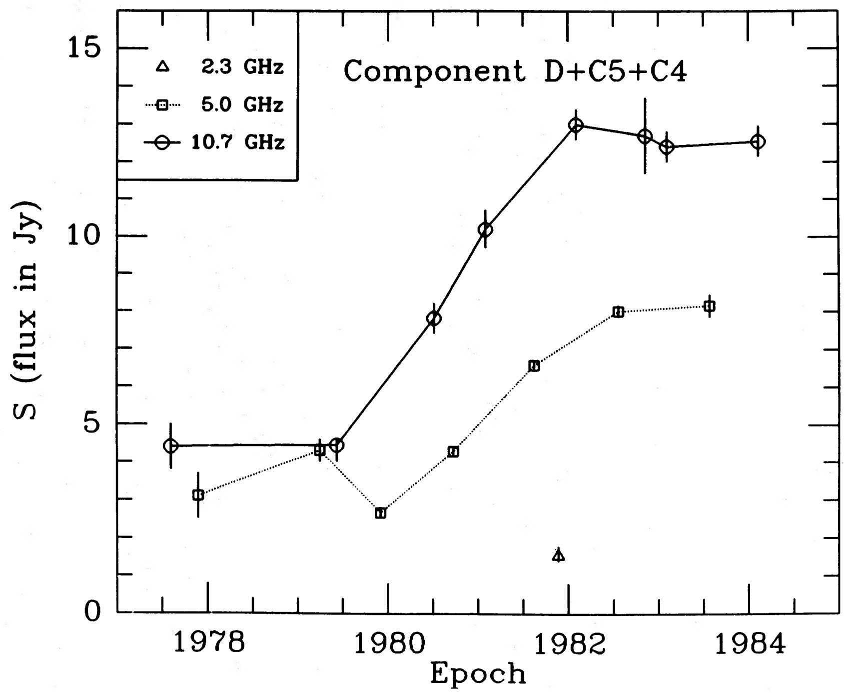

FIG. 6e

The sum of the fluxes of D and C5 appears to vary between 5 and 10 Jy at 22.2 GHz, and 4.5 to 7 Jy at 10.7 GHz (Fig. 6*d*). At 22.2 GHz the first and highest peak occurs in 1981; there is evidence for a second peak near or after 1984 which is due in part to C5. The 10.7 GHz data shows peaks at the same epochs. The spectral index between 5.0 and 10.7 GHz is 0.4 ± 0.2; between 10.7 and 22.2 GHz it varies from 0.22 to 0.54.

At 2.3 and 5.0 GHz components D, C5, and C4 are blended together at most epochs, so in Figure 6*e* we show the flux for the sum D+C5+C4. The large rise seen at 10.7 GHz beginning in 1979 is caused mostly by C4; it seems likely that it also causes the large rise seen at 5.0 GHz. The spectrum rises sharply between 2.3 and 5.0 GHz with $\alpha = 1.95 \pm 0.13$. Between 5.0 and 10.7 GHz the spectral index varies widely between 0.03 and 1.05.

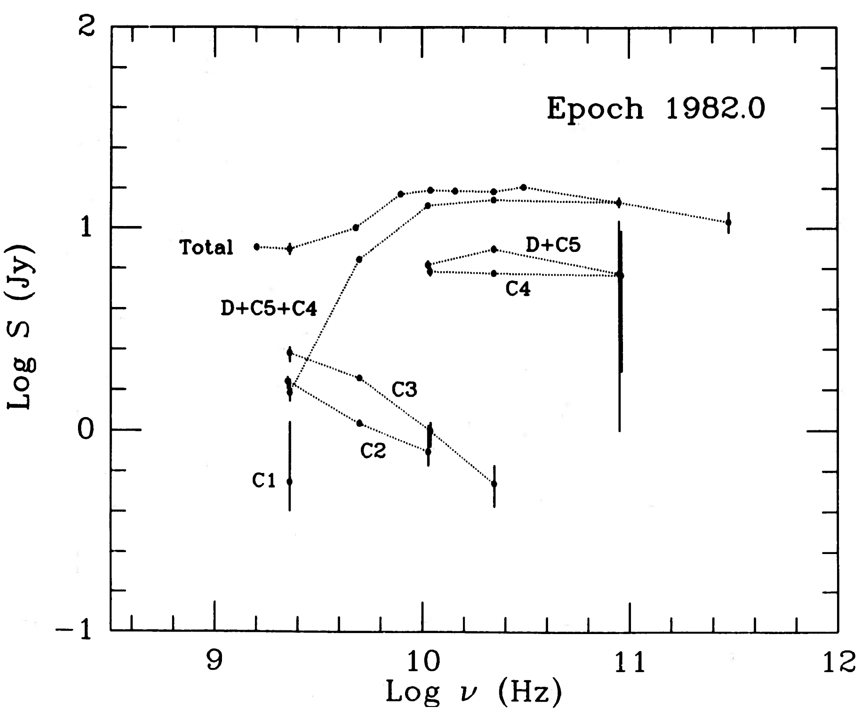

FIG. 7.—Fluxes components and total fluxes for epoch 1982.0

At epoch 1984.1 components D and C5 are resolved apart at 10.7 and 22.2 GHz. The spectral index of D between these frequencies is 0.30 ± 0.10.

c) *Counterjet/Jet Flux Ratio*

We estimate the counterjet/jet ratio using the 1983.57 epoch 5.0 GHz map. An annulus between 1.2 and 20.0 mas from the core was divided into eight equal octants with one centered on the jet at P.A. = $-85°$, and the flux in each octant was calculated. The background intensity level of the map was determined from the four octants closest to, but not containing, the counterjet (P.A. = 95°). The dispersion about the background level for these four octants was taken as the uncertainty for the flux in an octant. The jet and counterjet fluxes after background subtraction were 2.97 ± 0.02 Jy and -0.020 ± 0.022 Jy, respectively; hence, the counterjet/jet flux ratio is -0.007 ± 0.007. This is the smallest ratio yet reported for a compact radio source. This measured ratio does not appear to be biased by the starting model used in mapping. We obtained the same result even when the starting model had a counterjet/jet ratio of 0.1.

d) *Component Sizes*

Component diameters for C4, C3, and C2 are plotted against r in Figure 8. We may derive an opening angle for the source structure by fitting a line to these data. The observing frequency with the most complete data is 10.7 GHz; for this frequency the full opening angle is $25°.9 \pm 1°.6$, and the apex is at $r = -0.20 \pm 0.09$ mas. We have also taken the epochs with the best (u, v) coverage and fit separately for the component size along and perpendicular to the source axis. This produces an opening angle of $26°.7 \pm 2°.1$, in good agreement with the above value. This is much broader than opening angles for large-scale radio jets, which are typically a few degrees (Bridle and Perley 1984).

Each component also shows *direct* evidence for expansion. Expansion rates were derived by fitting straight lines to diameter ϕ versus epoch t with results given in Table 5. Expansion rates are in the range 0.04 to 0.15 mas yr^{-1}. The wide range may indicate the expansion is somewhat erratic on short time scales, or that the true errors are larger than the formal uncertainties we derive.

The values of $\phi(1982.0)$ in Table 5 indicate that the sizes of C2 and C4 do not depend on frequency. Component C3, however, appears to be $\sim 50\%$ larger at 5.0 than at 10.7 GHz. Simple opacity effects cannot explain this. A homogeneous sphere which is optically thick at 5.0 GHz and optically thin at 10.7 GHz would give a size ratio of ~ 1.2, which is much smaller than the observed ratio. Inhomogeneity in C3 could account for the observed size difference. Diameters for com-

TABLE 5

EXPANSION RATES $d\phi/dt$ FOR COMPONENTS AND SIZES $\phi(1982.0)$ FOR EPOCH 1982.0

Component	Frequency (GHz)	$d\phi/dt$ (mas yr^{-1})	$\phi(1982.0)$ (mas)
C2	5.0	0.17 ± 0.05	2.15 ± 0.08
	10.7	0.34 ± 0.26	2.4 ± 0.4
C3	5.0	0.15 ± 0.03	1.50 ± 0.05
	10.7	0.06 ± 0.03	0.97 ± 0.07
C4	10.7	0.10 ± 0.02	0.25 ± 0.03
	22.2	0.04 ± 0.01	0.29 ± 0.02

NOTE.—All measurements are in the observer's frame of reference.

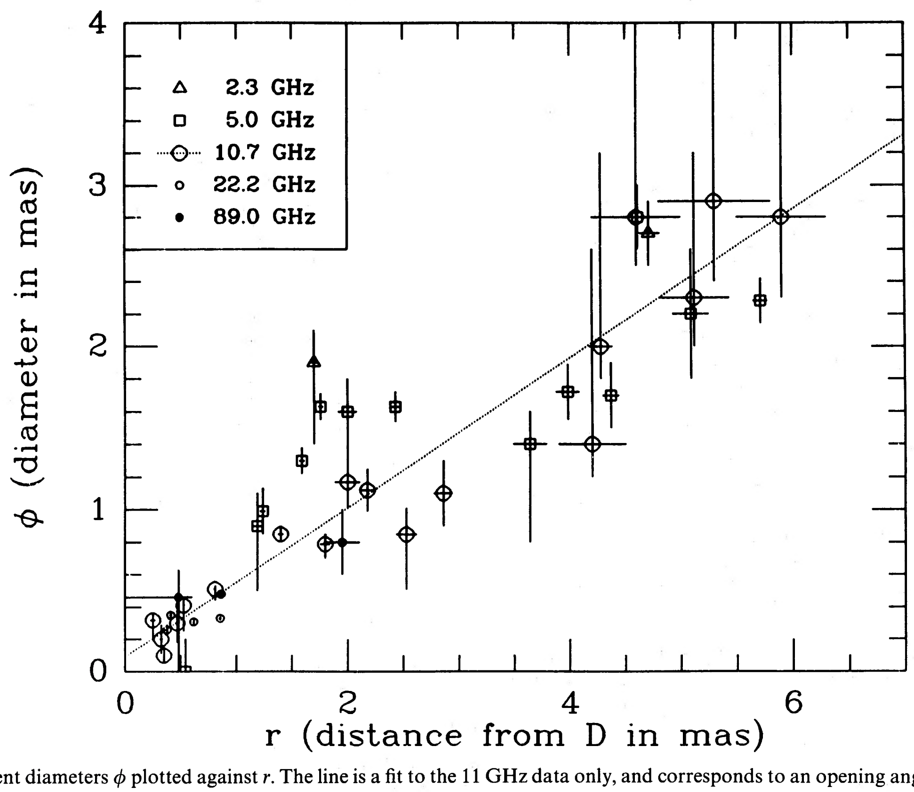

FIG. 8.—Component diameters ϕ plotted against r. The line is a fit to the 11 GHz data only, and corresponds to an opening angle of $25°.9 \pm 1°.6$.

ponent D tend to be around 0.3 mas at 10.7 and 22.2 GHz. At lower frequencies the diameters appear to be larger; we obtain 1.1 ± 0.3 and 1.6 ± 0.5 mas at 5.0 and 2.3 GHz, respectively. This effect may also be due to inhomogeneity.

V. SUMMARY

Important results may be summarized as follows:

1. A newly ejected knot C4 accelerates from ~ 0.07 to ~ 0.31 mas yr^{-1}. Older knots C3 and C2 have proper motions of 0.30 and 0.48 mas yr^{-1}, respectively, and show little or no acceleration.
2. While it was near the "core," knot C4 changed position angle from $-135°$ to $-87°$. Knots C3, C2, and C1 are at progressively larger position angles of $-86°$, $-74°$, and $-64°$, respectively. The "core" extension C5 has a P.A. $= -90°$, which suggests there may be no single track near the "core" which component centroids follow.
3. Distances from the "core" to the knots are larger at higher frequencies.
4. Knot C4 underwent a large flux outburst, increasing from ≤ 1 to ~ 8 Jy with a 2 yr time scale, then it began to decay with a 4 yr time scale. Its spectrum between 10.7 and 22.2 GHz remained flat during this time. Component C3 decays with a similar time scale, and its spectrum steepens.
5. The moving knots define an opening angle of $\sim 27°$ on the sky, and show direct evidence for expansion.
6. The ratio of the counterjet to jet flux density is -0.007 ± 0.007 at 5 GHz.

An interpretation of these data will appear in a separate article (Biretta *et al.* in preparation).

It is a pleasure to thank T. Pearson, A. Readhead, and S. Unwin for many useful discussions. L. Bååth and D. Backer, respectively, provided visibility data for the 1982.42 and 1982.38 epochs. This work was supported by grant AST82-10259 from the National Science Foundation. Observations at Haystack, Fort Davis, Owens Valley, and Hat Creek are supported by the NSF; NRAO is operated by Associated Universities, Inc., under contract with the NSF.

REFERENCES

Aller, H. D., and Aller, M. F. 1984, in *IAU Symposium 110, VLBI and Compact Radio Sources*, ed. R. Fanti, K. Kellermann, and G. Setti (Dordrecht: Reidel), p. 119.
Arndt, R. A., and MacGregor, M. H. 1966, *Nucl. Phys.*, **6**, 253.
Baars, J. W. M., *et al.* 1977, *Astr. Ap.*, **61**, 99.
Bååth, L. B., *et al.* 1981, *Ap. J. (Letters)*, **243**, L123.
———. 1986, in preparation.
Backer, D. 1984, in *IAU Symposium 110, VLBI and Compact Radio Sources*, ed. R. Fanti, K. Kellermann, and G. Setti (Dordrecht: Reidel), p. 31.
Bartel, N., *et al.* 1984, in *IAU Symposium 110, VLBI and Compact Radio Sources*, ed. R. Fanti, K. Kellermann, and G. Setti (Dordrecht: Reidel), p. 113.
Biretta, J. A. 1985, Ph.D. thesis, Caltech.
Biretta, J. A., Cohen, M. H., Unwin, S. C., and Pauliny-Toth, I. I. K. 1983, *Nature*, **306**, 42.
Bridle, A. H., and Perley, R. A. 1984, *Ann. Rev. Astr. Ap.*, **22**, 319.
Browne, I. W. A., *et al.* 1982*a*, *M.N.R.A.S.*, **198**, 673.
———. 1982*b*, *Nature*, **299**, 788.
Burbidge, E. M. 1965, *Ap. J. (Letters)*, **142**, 1674.
Clark, B. G. 1973, *Proc. IEEE*, **61**, 1242.
Cohen, M. H., *et al.* 1975, *Ap. J.*, **201**, 249.
———. 1976, *Ap. J. (Letters)*, **206**, L1.
———. 1983, *Ap. J.*, **272**, 383.
Cohen, M. H., and Unwin, S. C. 1984, in *IAU Symposium 110, VLBI and Compact Radio Sources*, ed. R. Fanti, K. Kellermann, and G. Setti (Dordrecht: Reidel), p. 95.
Cornwell, T. J. 1982*a*, in *Proc. NRAO-VLA Workshop, Synthesis Mapping*, ed. A. R. Thompson and L. R. D'Addario (Green Bank: NRAO), pp. 13-1–13-15.
———. 1982*b*, in *Proc. NRAO-VLA Workshop, Synthesis Mapping*, ed. A. R. Thompson and L. R. D'Addario (Green Bank: NRAO), pp. 9-1–9-14.
Cornwell, T. J., and Wilkinson, P. N. 1981, *M.N.R.A.S.*, **196**, 1067.
Feldman, P. A., MacLeod, J. M., and Andrew, B. H. 1981, *IAU Circ.*, No. 3637.
Grandi, S. A., and Tifft, W. G. 1974, *Pub. A.S.P.*, **86**, 873.
Hutchings, J. B., Crampton, D., and Campbell, B. 1984, *Ap. J.*, **280**, 41.
Ku, W. H.-M., Helfand, D. J., and Lucy, L. B. 1980, *Nature*, **288**, 323.
Linfield, R. 1981, *Ap. J.*, **244**, 436.
Marcaide, J., *et al.* 1984, in *IAU Symposium 110, VLBI and Compact Radio Sources*, ed. R. Fanti, K. Kellermann, and G. Setti (Dordrecht: Reidel), p. 247.
Moran, J. M. 1973, *Proc. IEEE*, **61**, 1236.
Moore, R. L., Readhead, A. C. S., and Bååth, L. L. 1983, *Nature*, **306**, 44.
Moore, R. L., and Stockman, H. S. 1981, *Ap. J.*, **243**, 60.
Mutel, R. L., and Phillips, R. B. 1984, in *IAU Symposium 110, VLBI and Compact Radio Sources*, ed. R. Fanti, K. Kellermann, and G. Setti (Dordrecht: Reidel), p. 117.
Neugebauer, G., *et al.* 1979, *Ap. J.*, **230**, 79.
Pearson, T. J., and Readhead, A. C. S. 1984, *Ann. Rev. Astr. Ap.*, **22**, 97.
Pollock, J. T., *et al.* 1979, *A.J.*, **84**, 1658.
Readhead, A. C. S., Hough, D. H., Ewing, M. S., Walker, R. C., and Romney, J. D. 1983, *Ap. J.*, **265**, 107.
Readhead, A. C. S., *et al.* 1978, *Nature*, **276**, 768.
Readhead, A. C. S., and Pearson, T. J. 1982, in *IAU Symposium 97, Extragalactic Radio Sources*, ed. D. S. Heeschen and C. M. Wade (Dordrecht: Reidel), p. 279.
Readhead, A. C. S., and Wilkinson, P. N. 1978, *Ap. J.*, **223**, 25.
Schilizzi, R. T., and de Bruyn, A. G. 1983, *Nature*, **303**, 26.
Simon, R. S. 1983, Ph.D. thesis, Caltech.
Unwin, S. C., Cohen, M. H., Pearson, T. J., Seielstad, G. A., Simon, R. S., Linfield, R. P., and Walker, R. C. 1983, *Ap. J.*, **271**, 536.
———. 1985, *Ap. J.*, **289**, 109.
Walker, R. C., *et al.* 1984, in *IAU Symposium 110, VLBI and Compact Radio Sources*, ed. R. Fanti, K. Kellermann, and G. Setti (Dordrecht: Reidel), p. 121.
Wittels, J. J., *et al.* 1976, *A.J.*, **81**, 933.

J. A. BIRETTA: Center for Astrophysics, 60 Garden St., Cambridge, MA 02138

M. H. COHEN: Caltech 105-24, Pasadena, CA 91125

R. L. MOORE: Aerospace Corp., Box 92957, Los Angeles, CA 90009